ROYAL SOCIETY OF CHEMISTRY

Check for updates

Electrochemical evaluation of Ni-BaZr$_{0.8}$Y$_{0.1}$X$_{0.1}$O$_{3-\delta}$ (X=Co, Mn) perovskite anodes synthesized through spinach (green) and oxalic (chemical) assisted auto-combustion routes for IT-SOFCs

Qurat ul Ain,[a] Muneeb Irshad, [ID] *[a] Muhammad Rafique, [ID] [b] Imen Kebaili[c] and Ali El-Rayyes [ID] [d]

The development of efficient and environmentally sustainable anode materials is essential for advancing solid oxide fuel cells (SOFCs). In this study, we introduced a pioneering green synthesis approach utilizing spinach leaves powder as a bio-derived chelating agent, alongside a conventional chemical route using oxalic acid, to synthesize Ni-BZr$_{0.8}$Y$_{0.1}$X$_{0.1}$O$_{3-\delta}$ (Ni-BZYX; X = Co, Mn) perovskite-based anodes. This eco-friendly method leverages natural, renewable spinach powder to reduce the environmental footprint of material synthesis, offering a sustainable alternative to traditional chemical processes. Structural characterization *via* XRD and FTIR confirmed the formation of single-phase cubic perovskite structures without secondary phases, demonstrating effective doping and phase stability in both synthesis routes. SEM analysis revealed that oxalic-acid-synthesized samples exhibited superior porosity, reduced particle agglomeration, and enhanced microstructural uniformity, facilitating efficient gas diffusion and expanding the electrochemically active triple-phase boundary (TPB). Electrochemical testing at 650 °C demonstrated that Ni-BZYCo (oxalic acid) delivered the highest power density of 0.56 W cm^{-2}. Although greenly synthesized anodes exhibited slightly lower performance due to minor residual impurities, the spinach-based approach represents a significant advancement toward sustainable SOFC materials with comparable structural and functional properties. This work underscores the environmental and practical potential of bio-derived synthesis strategies and positions Co-doped Ni-BZY as a high-performance anode for sustainable SOFC technologies.

1 Introduction

A significant portion of global energy demand continues to be met through the consumption of fossil fuels, a practice that contributes extensively to greenhouse gas emissions and the escalation of climate-related concerns. In response to the urgent need for sustainable and cleaner alternatives, solid oxide fuel cells (SOFCs) have emerged as a promising solution for eco-friendly power generation. This device converts chemical energy directly into electricity with high efficiency and minimal pollutant release, particularly when fueled by hydrogen or renewable bio-based sources.[1–6]

To enhance the practicality and commercial viability of SOFC technology, considerable efforts are directed toward lowering the operational temperature to an intermediate range of 400–700 °C. Such a temperature reduction is desirable because it can decrease material degradation, extend device lifespan, and reduce overall manufacturing costs.[7] Adopting protonic ceramic fuel cells (PCFCs) is a compelling approach to achieving these benefits. PCFCs represent a promising technology for converting chemical energy into electricity, offering high efficiency and minimal environmental impact.[8–12] These fuel cells utilize proton-conducting electrolytes, typically based on acceptor-doped perovskite oxides such as BaCeO$_3$, BaZrO$_3$. These materials are particularly attractive for intermediate-temperatures SOFC applications (400–700 °C) due to their superior proton conductivity compared to traditional oxide-ion conducting electrolytes. A notable advantage of PCFCs is their ability to operate on a diverse range of fuels, including hydrogen, hydrocarbons, methanol, and ammonia, making them highly adaptable for various energy systems. Unlike conventional oxygen-ion-conducting SOFCs, PCFCs transport protons

[a]Department of Physics, University of Engineering and Technology, Lahore 54890, Pakistan. E-mail: muneebirshad@gmail.com; muneeb_irshad@uet.edu.pk

[b]Department of Physics, University of Sahiwal, Sahiwal 57000, Pakistan

[c]Department of Physics, Faculty of Science, King Khalid University, Abha, Saudi Arabia

[d]Center for Scientific Research and Entrepreneurship, Northern Border University, Arar 73213, Saudi Arabia

through the electrolyte and generate water at the cathode. This cathode-side water formation not only improves thermal management and reaction kinetics but also prevents fuel dilution, thereby enhancing fuel utilization and system efficiency.[9,13,14]

Several anode materials have been explored for application in protonic ceramic fuel cells (PCFCs), including Ni-based composites such as Ni-BCY, Ni-BZY, and other formulations incorporating combinations like Ba(Ce, Zr, Y, Yb)$O_{3-\delta}$, SrCe$_{0.9}$Yb$_{0.1}$O$_{3-\delta}$, Ca(Zr,Y)$O_{3-\delta}$, and Sr(Zr, Y)$O_{3-\delta}$.[15–20] Among these, Ni-BCY has been widely studied due to its high proton conductivity. However, its performance is significantly compromised in environments containing water vapor and carbon dioxide, as the material is prone to decomposition under such conditions.[21] This limitation poses challenges for its use with hydrocarbon or biomass-derived fuels. In contrast, Ni-BZY-based cermets exhibit superior thermochemical stability in H_2O- and CO_2-rich atmospheres, making them a more robust and viable choice for long-term operation in practical PCFC applications, particularly when alternative carbon-containing fuels are used. The electrochemical performance of PCFC cermet anodes can be effectively tuned by adjusting parameters such as the nickel content, the protonic conductivity of the ceramic matrix, and the overall porosity of the composite structure.[22,23]

To attain optimal electrochemical performance in fuel cells, anode cermets must exhibit an extensive triple-phase boundary (TPB). However, redox cycling, repeated exposure to oxidizing and reducing atmospheres, can significantly compromise the TPB length and integrity. In the case of Ni-YSZ anodes, widely used in oxygen-ion-conducting SOFCs, the redox processes have detrimental effects on the microstructure.[24] It has been observed that the original microstructural arrangement and phase distribution often fail to fully recover after cycles of oxidation and subsequent reduction.[24–26] The mechanical and electrochemical durability of such anodes is closely linked to their internal structure and the distribution of metallic and ceramic phases within the cermet.[27] Research findings consistently show that Ni-YSZ anodes are particularly vulnerable to redox-induced degradation, with the deterioration rate accelerating under low-porosity conditions. The oxidation of metallic Ni to NiO results in a significant volume expansion, which can generate internal stresses, causing microcracks and delamination at the electrode–electrolyte interface. These structural disruptions severely hinder electrochemical activity and contribute to rapid performance loss in fuel cell systems.[28–30]

Due to persistent challenges such as carbon fouling, sulfur contamination, and redox instability associated with traditional anode materials when exposed to various fuels, there has been growing interest in exploring oxide-based alternatives.[19] These oxides are generally classified by their crystal structures, including fluorite, pyrochlore, tungsten bronze, rutile, and perovskite types. Among these, perovskite-structured oxides have garnered significant attention as viable anode candidates. This is attributed to their excellent redox tolerance, satisfactory electrical and ionic conductivity, and strong catalytic activity for fuel reforming, along with their resilience against sulfur and carbon-based contaminants.[19,20] Perovskite materials often function as mixed ionic-electronic conductors (MIECs), enabling abundant oxygen vacancies within the lattice. These vacancies enhance oxide ion transport and facilitate more efficient fuel oxidation reactions at the anode interface. A key advantage of MIECs lies in their ability to expand the electrochemically active triple-phase boundary (TPB) from a narrow interface at the electrolyte to a broader region extending throughout the anode surface. This expanded TPB region offers a greater number of active sites for electrochemical reactions, which can significantly boost fuel oxidation kinetics and overall anode performance.[31–34]

Composite and doping strategies have thus gained attention. In particular, B-site substitution of perovskite oxides with active transition metals (Co, Mn, Ni, Cu, Zn, *etc.*) can introduce variable-valence states and oxygen vacancies that boost mixed electronic/ionic conduction and catalytic oxidation activity.[35–37] The selection of cobalt (Co) and manganese (Mn) as B-site dopants for anodes was driven by their ability to enhance mixed ionic–electronic conductivity, catalytic activity, and structural stability. Co and Mn, with variable valence states (Co^{2+}/Co^{3+}, $Mn^{2+}/Mn^{3+}/Mn^{4+}$), introduce oxygen vacancies that improve ionic transport and expand the triple-phase boundary, facilitating efficient fuel oxidation.[31,35] Their catalytic properties enhance reaction kinetics, particularly for hydrogen and hydrocarbon fuels.[19,20] Additionally, their ionic radii (Co^{3+}: 0.61 Å; Mn^{3+}: 0.66 Å) ensure compatibility with the BaZrO$_3$ lattice, maintaining a single-phase cubic structure (*Pm3m*) while inducing beneficial lattice distortion.[16,38] Co and Mn also act as sintering aids, improving microstructure and conductivity under reducing conditions. Thus, Co/Mn-substituted perovskites generally exhibit higher conductivity and redox stability than undoped oxides.[16,39,40]

The present study targets B-site (Co- and Mn) doped Ni-BZY anodes with composition BaZr$_{0.8}$Y$_{0.1}$X$_{0.1}$O$_{3-\delta}$ (X = Co, Mn). We employed an eco-friendly auto-combustion route using spinach dry leaves powder as a bio-chelating agent and oxalic acid as a chemical chelating agent to synthesize the powders.

Spinach leaves powder was selected as the green chelating agent due to its rich organic composition, environmental sustainability, and compatibility with the synthesis process. Spinach contains natural chelating compounds, such as oxalic acid, polyphenols, flavonoids, *etc.*, which effectively chelate complex metal cations, ensuring homogeneous phase formation, as confirmed by XRD analysis.[41] Its renewable, biodegradable nature aligns with green chemistry principles, reducing the environmental footprint compared to synthetic agents like oxalic acid.[42] Additionally, spinach's high organic content provides exothermic energy for auto-combustion, facilitating perovskite phase formation at low temperatures.[41] This novel use of spinach can advance sustainable SOFC material synthesis, leveraging its abundance, low cost, and ease of preparation.

The Ni-BZYX (X = Co, Mn) perovskite anodes, synthesized *via* green (spinach leaves powder) and chemical (oxalic acid) auto-combustion routes, were characterized to evaluate the impact of Co and Mn B-site doping and synthesis method on their

structural and electrochemical properties. Structural analysis (XRD, SEM) confirmed phase purity and microstructural features, while functional characterization (FTIR) verified chemical bonding. Electrical conductivity and electrochemical performance in IT-SOFC conditions were measured to assess the effects of doping and synthesis routes, providing insights into the viability of the green synthesis approach for sustainable, high-performance anode development.

2 Experimentation

Ni-BaZr$_{0.8}$Y$_{0.1}$X$_{0.1}$O$_{3-\delta}$ (Ni-BZYX), incorporating transition metals as B-site co-dopants (X = Co, Mn) for use as SOFC anode, was synthesized *via* an auto-combustion method. The synthesis process employed two distinct chelating agents: oxalic acid and spinach leaves powder in dry powder form. The stoichiometric aggregate of barium nitrate (Ba(NO$_3$)$_2$, UNI-CHEM, 99.95% purity), zirconium nitrate pentahydrate (Zr(NO$_3$)$_4 \cdot$5H$_2$O, Sigma-Aldrich, 99.99% pure), yttrium nitrate hexahydrate (Y(NO$_3$)$_3 \cdot$6H$_2$O, Sigma-Aldrich, 99.99% pure), manganese nitrate dihydrate (Mn(NO$_3$)$_2 \cdot$2H$_2$O, UNI-CHEM, 99.95% purity), and cobalt nitrate hexahydrate (Co(NO$_3$)$_2 \cdot$6H$_2$O, UNI-CHEM, 99.95% purity) were continuously mixed in distilled water at 80 °C for 30 minutes using a magnetic stirrer on a hot plate. The mixture was then stirred and heated to 120 °C for an additional 60 minutes to obtain a homogeneous solution. Subsequently, an aqueous solution containing 40 wt% nickel nitrate hexahydrate (Ni(NO$_3$)$_2 \cdot$6H$_2$O, UNI-CHEM, 99.95% purity) was added to this solution and stirred for an additional 30 minutes to ensure uniformity. 20 wt% oxalic acid was added as a chemical chelating agent to this homogeneous solution. The homogeneous solution was further stirred continuously at 80 °C, resulting in the formation of a gel that gradually underwent self-combustion, yielding a fine powder. This powder was then sintered at 1200 °C for six hours. After cooling to room temperature, the resulting precursor powder was ground using a mortar and pestle to achieve a fine and uniform consistency.

Another homogenous solution was made using the same stoichiometric amount of nitrate and a different chelating agent (20 wt% spinach dry powder). The homogeneous mixture was
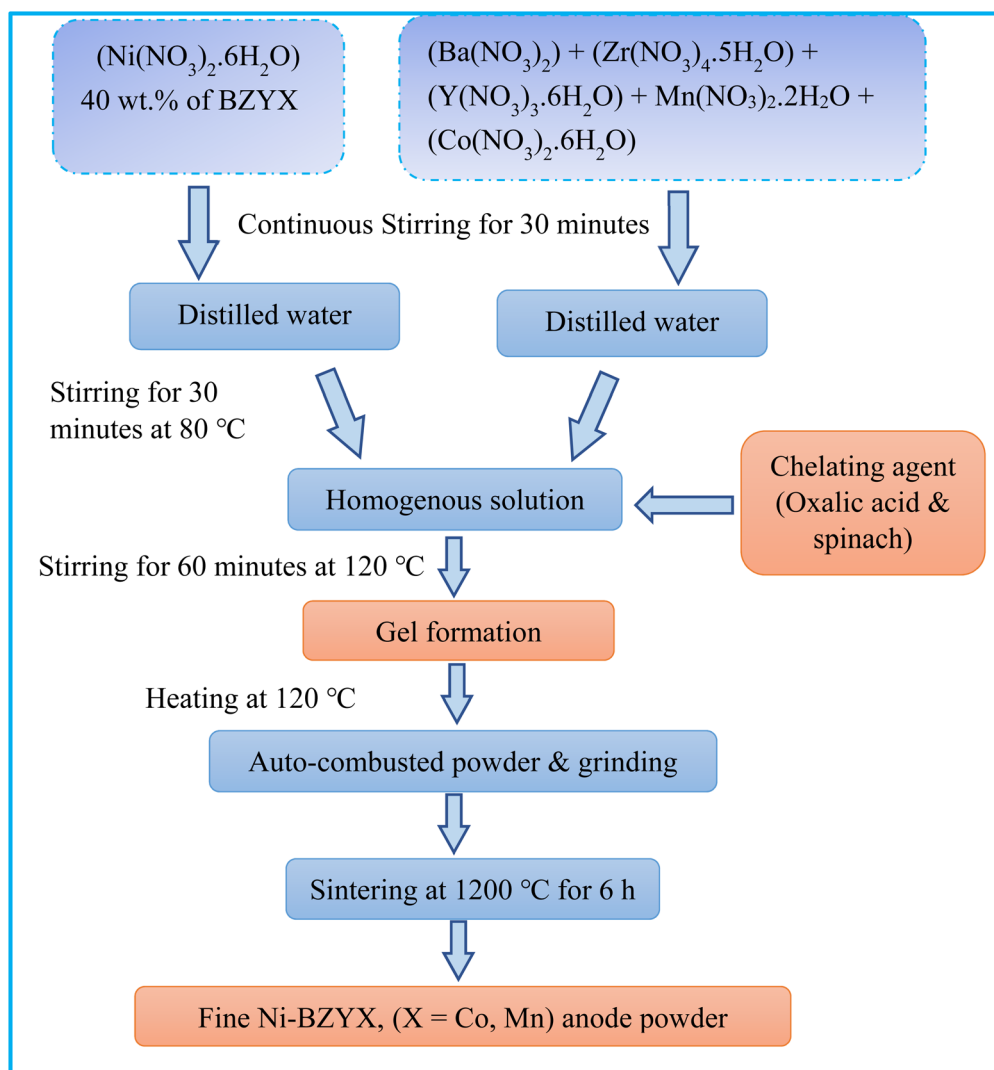

Fig. 1 Flow chart for the Ni-BaZr$_{0.8}$Y$_{0.1}$X$_{0.1}$O$_{3-\delta}$ (Ni-BZYX, X = Co, Mn) anode synthesis.

stirred again for 30 minutes at 80 °C, followed by 60 minutes at 120 °C. This process resulted in the formation of a gel that spontaneously combusted into a powder. The obtained powder samples were subsequently sintered at 1200 °C for 6 hours. Following natural cooling to room temperature, the synthesized powders were finely ground using a mortar and pestle to ensure uniformity. This same procedure was applied consistently for the synthesis of all samples (Fig. 1).

2.1 Cell fabrication

The overall electrochemical performances of cells having Ni-BZYX (X = Co, Mn) anodes, synthesized with two different chelating agents, *i.e.*, oxalic acid and spinach leaves powder, were assessed by fabricating 13 mm diameter pellets under a pressure of 200 MPa through a hydraulic press. BZY served as the electrolyte, while BSCF was utilized as the cathode. During testing, saturated hydrogen (~3% H_2O) at a flow rate of 50 mL min^{-1} was provided as the fuel to the anode, while oxygen was supplied as an oxidant at the cathode.

3 Results and discussions

3.1 Structural analysis

Fig. 2 depicts the XRD spectra of Ni-BZYX (X = Co and Mn) SOFC anode, synthesized utilizing various chelating agents, namely oxalic acid and spinach leaves powder, within the Bragg angle range of $2\theta = 20°–80°$.

The diffraction planes at (110), (111), (200), (211), (220), (310), (311), and (222) correspond to the BZY with primitive space group of *Pm3m* (ICDD # 980107880)[35,38] and (111), (200) (220), (311), and (222) correspond to the NiO (JCPD card no. 01-1239)[43] confirming the development of cubic perovskite

configuration of all the synthesized materials. The absence of secondary phases confirms the successful incorporation and solubility of transition metals (Mn, Co) within the host lattice, regardless of whether the synthesis was conducted through chemical or green routes. The presence of distinct BZYX and NiO peaks in the diffractogram and the absence of secondary phases indicate that no chemical reactions occur during synthesis.

The variation in ionic radii between the host element (Zr^{4+}, r = 0.72 Å) and the dopant (Y^{3+}, r = 0.9 Å) results in a peak shift in BZY towards lower angles compared to pure barium zirconate, which exhibits a prominent diffraction peak at $2\theta = 30$.[44] In this study, the observed peak shift occurs at $2\theta = 30.17°$ for the (110) plane of BZYMn synthesized with spinach and oxalic acid, while for BZYCo (oxalic acid) and BZYCo (spinach), the peak shift is noted at $2\theta = 30.21°$. The displacement of the peak to a higher angle than BZY indicates a reduction in lattice parameters due to lattice contraction. This contraction is attributed to the incorporation of secondary dopants with smaller ionic radii, such as Co^{3+} (0.61 Å) and Mn^{3+} (0.66 Å), in place of the larger Zr^{4+} (0.72 Å) and Y^{3+} (0.9 Å). The average crystallite sizes of BZYX (X = Co, Mn) synthesized utilizing spinach and oxalic acid were determined using the Scherrer formula, given in eqn (1).

$$D = \frac{K\lambda}{\beta \cos\theta} \quad (1)$$

The parameter K, commonly assigned a value of 0.9, represents the shape factor. The symbol λ denotes the X-ray wavelength (λ = 0.15406 nm), while β corresponds to the full width at half maximum (FWHM), and the diffraction angle is symbolized as θ. The average crystallite sizes of Ni-BZYCo (spinach), Ni-BZYCo (oxalic acid), Ni-BZYMn (spinach), and Ni-BZYMn (oxalic acid)
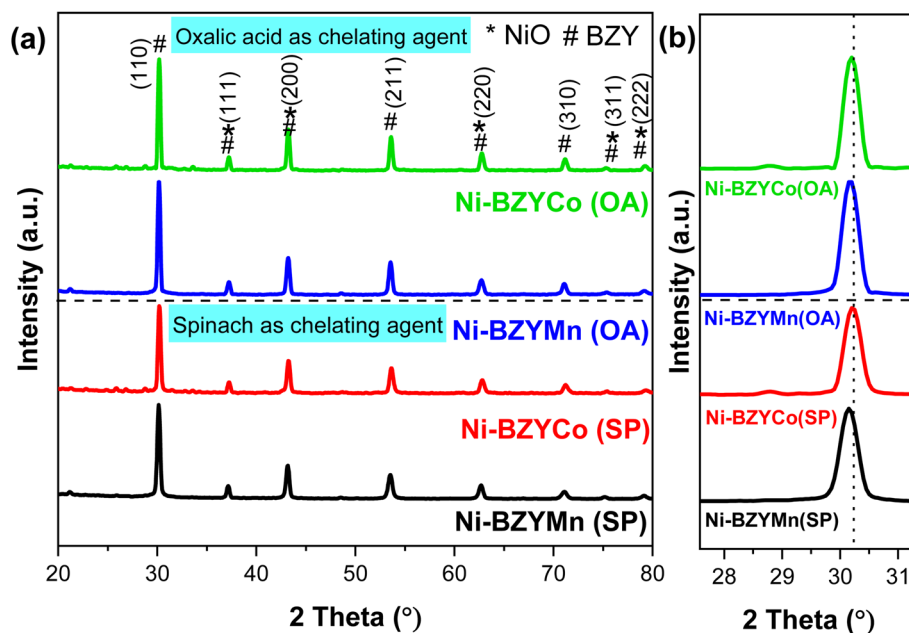

Fig. 2 XRD spectra of Ni–BZYX (X = Co, and Mn) SOFC's anode synthesized by utilizing spinach (SP) and oxalic acid (OA) as chelating agents (a) and enlarged (110) plane (b).

Table 1 The average crystallite sizes of Ni–BZYX (X = Co, and Mn) synthesized materials using oxalic acid (OA) and spinach powder (SP) as chelating agents

Materials	Dopants	Crystallite size (nm)
Ni-BZYX (SP)	Mn	19.55
Ni-BZYX (OA)	Mn	22.27
Ni-BZYX (OA)	Co	26.04
Ni-BZYX (SP)	Co	21.94

are 21.94 nm, 26.04 nm, 19.55 nm, and 22.27 nm, respectively (Table 1).

3.2 Surface morphological analysis

Fig. 3 depicts the SEM micrographs of Ni-BZYX (X = Co, and Mn) SOFC's cermet anode utilizing various chelating agents, namely oxalic acid and spinach leaf powder.

SEM micrographs reveal that samples synthesized with oxalic acid (Ni-BZYCo (OA) and Ni-BZYMn (OA)) exhibit higher porosity and reduced particle agglomeration compared to those synthesized with spinach leaves powder (Ni-BZYCo (SP) and Ni-BZYMn (SP)). While the formation of NiO during sintering, acting as a sintering aid, contributes to densification in all

samples,[36,40,45] the choice of chelating agent further influences the microstructure. Oxalic acid enhances cation solubility and solution homogeneity, promoting a well-connected, porous particle network that facilitates gas diffusion and enhances TPB reactivity. In contrast, spinach-synthesized samples show denser morphologies, likely due to residual metallic impurities in the spinach powder that promote particle agglomeration.[42] However, pre-reduction of NiO to Ni metal in a hydrogen-rich atmosphere during SOFC operation can increase porosity by creating gas diffusion channels, potentially improving TPB accessibility and electrochemical performance, particularly for denser spinach-synthesized samples.[23,24]

Among the synthesized samples, those prepared using oxalic acid are expected to exhibit higher reactivity at the TPB due to their enhanced porosity and well-connected particle network. This structural advantage facilitates better gas diffusion and charge transfer, ultimately improving overall performance.[46]

The ionic radii difference between host (Zr) and dopants (Mn, Co) ions caused structural disorder which results in particle agglomeration. Because Mn and Zr have smaller ionic radius differences, which causes lesser structural distortions and hence the formation of comparative dense structure.[41] The micrographs of Ni-BZYMn reveal a denser morphology compared to Ni-BZYCo, irrespective of the chelating agent used
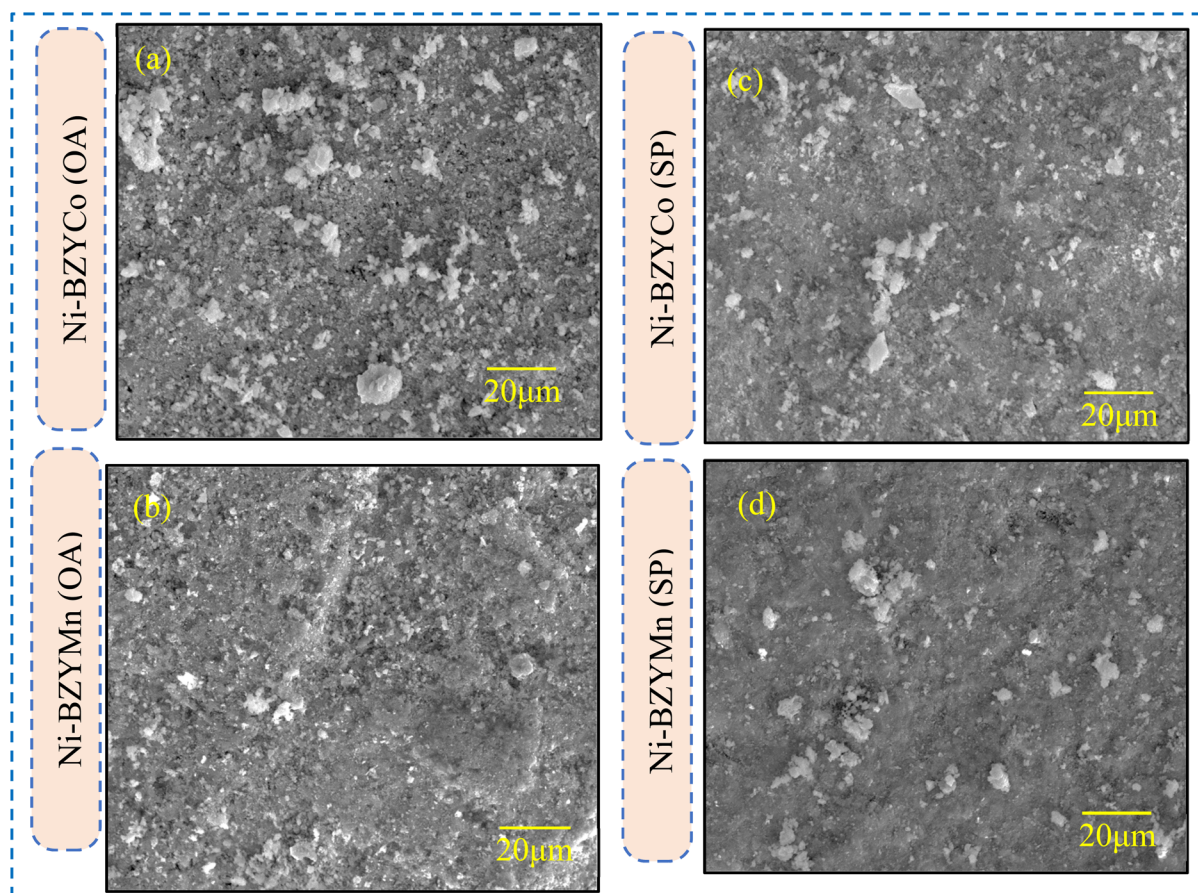

Fig. 3 SEM micrographs of Ni–BZYX (X = Co, and Mn) SOFC's anode synthesized by chemical (oxalic acid, OA) (a and b) green (spinach, SP) (c and d) route.

(oxalic acid or spinach). However, Ni-BZYMn synthesized with spinach exhibits greater agglomeration, likely due to the presence of metallic impurities in spinach that causes agglomeration. In contrast, oxalic acid helps minimize agglomeration during heat treatment, enhances cation solubility, and ensures better homogeneity of the solution, leading to improved structural uniformity.[42]

The micrographs of Ni-BZYCo synthesized using oxalic acid and spinach exhibit higher porosity and reduced agglomeration compared to Ni-BZYMn synthesized with the same chelating agents. It is well-recognized that surface area and porosity are key factors in improving SOFC performance. As electrochemical reactions primarily occur at the TPBs, the dense microstructure of Ni-BZYMn (oxalic acid and spinach) and Ni-BZYCo synthesized with spinach may hinder gas diffusion toward the TPB, potentially limiting performance. In contrast, Ni-BZYCo synthesized with oxalic acid, due to its porous and well-interconnected particle network, is expected to exhibit higher reactivity at TPBs compared to other samples, thereby improving electrochemical performance and making it a promising material for SOFC anodes.

3.3 Spectroscopic analysis

Fig. 4 represents the FTIR absorption peaks for Ni-BZYX (X = Co, and Mn) SOFC anode, utilizing various chelating agents *i.e.* dry spinach leaves powder and oxalic acid in 4000–450 cm^{-1} wavenumber range.

The absorption peaks in the range 1700–1400 cm^{-1} and 3800–3200 cm^{-1} occur due to O–H bending and stretching, respectively. These bands depict water adsorption into the lattice, possibly due to air or moisture. The absorption peaks at 2981, and 2340 cm^{-1} are associated with C–H stretching vibration and the peak at 1061 cm^{-1} is attributed to C–H bending vibration.[47] The absorption bands within the 1400–1100 cm^{-1} range indicate the presence of metal–oxygen–metal

(M–O–M) bonds, including Ba–O–Ba, Co–O–Co, Mn–O–Mn, and similar structural linkages.[48] The absorption peaks observed in the 770–850 cm^{-1} range correspond to C=C bending vibrations, characteristic of the alkene functional group. The bands at about 1598 and 1560 cm^{-1} correspond to the carbonate absorption bands.[49] This shows that carbonate species remained in all samples even after the sintering. The band around 686 cm^{-1} corresponds to the asymmetric stretching mode of metal–oxygen bond (O–Mn or Co–O) bonds.[50] These characteristic peaks further validate the presence of a perovskite structure and are associated with the vibrational modes of the B-site cation, specifically zirconium (Zr). The observed vibrational frequencies indicate the interaction of Zr within the perovskite lattice, confirming its successful incorporation and structural stability.[51] The absorption peaks observed near 530 cm^{-1} are attributed to the Ni–O vibrational stretching mode, indicating the presence of nickel oxide within the material's structure.[52] Therefore, the FTIR spectrum confirms the formation of NiO particles, which is consistent with the XRD findings.

There is no peak shifting or change in the peak intensity, which indicates the ordered structure of all the synthesized samples irrespective of the utilization of different chelating agents.

3.4 Conductivity

Fig. 5 represents the Arrhenius plot showing the relation between conductivity and temperature for Ni-BZYX (X = Co, and Mn) SOFCs' anode synthesized by two chelating agents, *i.e.*, green (spinach) and chemical (oxalic acid), within temperatures range of 300–800 °C, under Hydrogen–Argon atmosphere.

The data shows that all anodes have considerable conductivities, irrespective of the synthesis method and dopants. This effect is attributed to the incorporation of Co and Mn as sintering aids, which lower the sintering temperature while
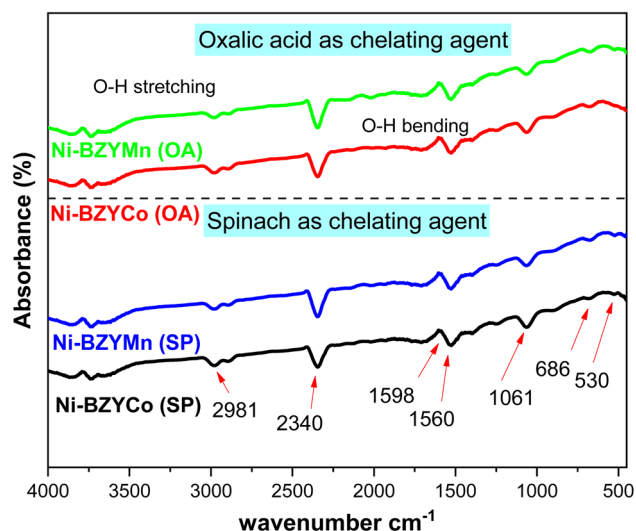

Fig. 4 FTIR Spectra of Ni-BZYX (X = Co, and Mn) SOFC's anode synthesized by using spinach (SP) and oxalic acid (OA) as chelating agents.
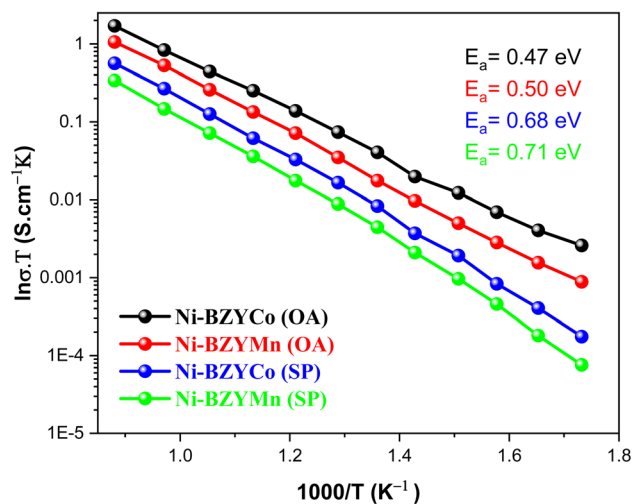

Fig. 5 Conductivity of Ni-BZYX (X = Co, and Mn) SOFC'S anode synthesized utilizing spinach powder (SP) and oxalic acid (OA) as chelating agents.

enhancing conductivity, as reported in previous studies.[40] Moreover, conductivity exhibits an increasing trend at elevated temperatures and declines as the temperature decreases, likely due to the formation of oxygen vacancies at higher temperatures.

The conductivity plot demonstrates that Ni-BZYMn (OA) and Ni-BZYCo (OA) exhibit superior conductivity compared to SOFC anodes synthesized using spinach powder as a chelating agent. This enhanced performance can be ascribed to the improved purity and better cation solubility facilitated by oxalic acid during synthesis. In contrast, the lower conductivity observed in Ni-BZYMn (SP) and Ni-BZYCo (SP) can be associated with the presence of metallic impurities inherent in spinach leaves powder. These impurities, in combination with the dopants (X = Co, Mn), may have adversely affected the ionic transport pathways, thereby reducing overall conductivity. Furthermore, the materials synthesized using spinach leaves powder may exhibit lower cation solubility and hindered crystallization, leading to the crystal structure's defects or irregularities. Such structural inconsistencies can disrupt charge transport mechanisms, resulting in a significant drop in ionic conductivity.[53] The higher conductivity observed in Ni-BZYCo may be due to the significant ionic radii difference between Co and Zr compared to Mn. This disparity induces greater lattice distortion within the crystal structure, leading to an increased level of disorder in the material. Such structural modifications influence the electronic configuration, thereby altering the charge transport dynamics. The enhanced lattice distortion promotes the creation of more oxygen vacancies, which act as active sites for ion migration. Additionally, the increased disorder disrupts the regular arrangement of atoms, facilitating the movement of charge carriers and ultimately improving electron transport throughout the material. This synergistic effect of structural deformation and improved charge carrier mobility contributes to the superior conductivity exhibited by Ni-BZYCo compared to its Mn-doped counterpart.[54]

3.5 Electrochemical performance

Fig. 6 depicts the electrochemical performance at 650 °C of four button cells synthesized Ni-BZYX (X = Co, and Mn) SOFC anode with spinach leaves powder and oxalic acid as chelating agents. Pellets with a diameter of 13 mm and 1.5 mm thickness, approximately, were manufactured using a uniaxial press under pressure of around 200 MPa to fabricate button cells. To prevent breakage and minimize potential losses, nickel foil was applied to the anode side. Humidified hydrogen ($\sim$3% H_2O) was delivered to the anode as fuel at a regulated flow rate of 50 mL min^{-1}, while oxygen was utilized as the oxidant at the cathode.

The Ni-BZYX (X = Co, Mn) anodes synthesized using oxalic acid exhibited peak power densities of 0.56 W cm^{-2} and 0.53 W cm^{-2}, with corresponding OCV of 0.91 V and 0.90 V, respectively. Notably, Ni-BZYCo (OA) achieved a maximum power density of 0.56 W cm^{-2} with an OCV of 0.91 V. The superior performance can be attributed to the improved TPB and the optimized structure porosity, which contribute to enhanced electrochemical activity and charge transport.[49] The SEM
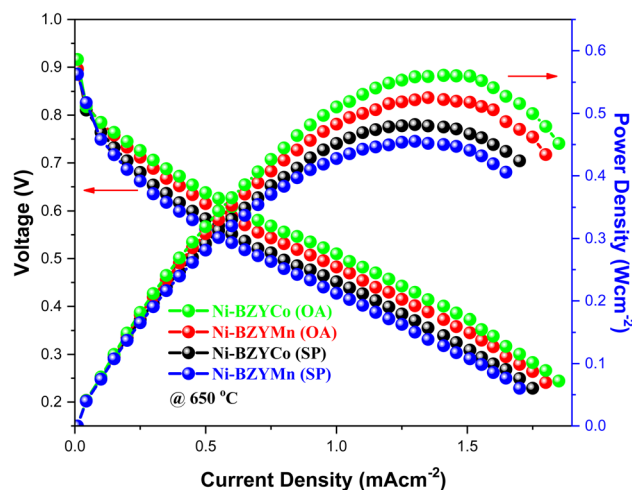

Fig. 6 Electrochemical evaluation of Ni-BZYX (X = Co, and Mn) SOFC's Anode synthesized by using spinach (SP) and oxalic acid (OA) as chelating agents.

micrograph revealed a well-developed microstructure of Ni-BZYCo (OA) and its appropriate porosity. Its high performance can be attributed to large oxygen vacancies with a maximum trapping effect, substantial charge compensation, and enhanced oxygen reduction reaction.[53] A higher degree of crystallinity contributes to a more ordered crystal structure, which can enhance the transport pathways for both oxygen ions and electrons, ultimately improving the performance of the SOFC. Additionally, the Ni-BZYCo anode synthesized using oxalic acid exhibited superior performance, as a highly crystalline structure provides a well-defined surface that enhances catalytic activity and reduces polarization resistance. This improved crystallinity leads to better electrochemical properties, facilitating more efficient charge transfer and reaction kinetics within the fuel cell.

The Ni-BZYCo and Ni-BZYMn anodes synthesized using spinach leaves powder exhibit power densities of 0.47 W cm^{-2} and 0.44 W cm^{-2}, with corresponding OCV of 0.89 V and 0.88 V, respectively. The Ni-BZYCo and Ni-BZYMn anodes synthesized using spinach leaf powder exhibit lower power densities (0.47 W cm^{-2} and 0.44 W cm^{-2}, respectively) compared to their oxalic-acid-synthesized counterparts (0.56 W cm^{-2} and 0.53 W cm^{-2}, respectively). This performance difference is partly attributed to the denser microstructure of spinach-synthesized samples, which may hinder gas diffusion to the TPB due to residual impurities such as potassium, calcium, iron, *etc.* present in spinach powder and increased agglomeration.[42] These impurities may introduce lattice distortions or secondary phases that disrupt ionic and electronic transport pathways.[53] In contrast, oxalic acid promotes a more porous microstructure and higher cation solubility, enhancing TPB reactivity and charge transport.[42,49] However, during SOFC operation, pre-reduction of NiO to Ni metal in a hydrogen-rich atmosphere can enhance porosity by forming gas diffusion channels, potentially improving TPB accessibility and electrochemical performance.[23,24] The superior

performance of oxalic-acid-synthesized Ni-BZYCo (0.56 W cm^{-2}, OCV 0.95 V) is attributed to its optimized porosity, enhanced oxygen vacancy concentration, and improved charge transport, as confirmed by SEM and conductivity analyses.[49,53] The superior power density of Ni-BZYCo in both sets can also be attributed to its distinct microstructural characteristics. SEM micrographs reveal that it possesses moderate porosity compared to other samples, which facilitates improved gas diffusion and enhances electrochemical reactions at the triple-phase boundary,[55] thereby increasing the overall performance. Ni-BZYMn (spinach) has lower power density due to the increased content of Mn in spinach, which acts as a secondary phase and reduces the overall performance. Based on the electrochemical performance, all Ni-BZYX (X = Co, Mn) anodes demonstrate suitability for IT-SOFC applications, with the oxalic-acid-synthesized anodes exhibiting superior power density and the spinach-based green synthesis method showing promising potential that can be further enhanced through optimization of microstructure and impurity reduction.

4 Conclusion

Ni–BZr$_{0.8}$Y$_{0.1}$X$_{0.1}$O$_{3-\delta}$ (Ni-BZYX, X = Co, Mn) perovskite anodes with B-site transition metal sintering aids have been successfully synthesized for the first time using a sustainable method incorporating spinach powder as a chelating agent. This environmentally friendly synthesis approach preserves the essential properties required for SOFC anode applications without significant compromise. XRD analysis confirmed the formation of a cubic perovskite structure, with no significant secondary phases detected, apart from minor shifts attributed to variations in ionic radii between dopants, the host matrix, and residual impurities. FTIR further verified the presence of a well-structured perovskite phase. SEM analysis revealed a uniformly distributed porous structure. Conductivity assessments demonstrated that chemically synthesized Ni-BZYX (X = Co, Mn) anodes exhibited superior electrical properties compared to their green-synthesized counterparts. Among the tested compositions, the Ni-BZYCo anode achieved the highest conductivity in both synthesis approaches, indicating its enhanced charge transport capability. Electrochemical performance measurements further confirmed the effectiveness of this synthesis method, with the Ni-BZYCo anode produced *via* the sustainable approach achieving a maximum power density of 0.47 W cm^{-2}. These findings demonstrate the viability of the novel, eco-friendly spinach-based synthesis route for producing high-performance Ni-BZYX (X = Co, Mn) perovskite anodes, achieving power densities close to that of chemically synthesized counterparts (0.47 W cm^{-2} *vs.* 0.56 W cm^{-2} for Ni-BZYCo). The slightly lower performance of spinach-synthesized anodes is attributed to denser microstructures and residual metallic impurities (*e.g.*, K, Ca, Fe) that promote agglomeration and reduce conductivity. Future optimization, such as impurity reduction through pre-treatment of spinach powder or enhanced combustion processes, could further close the performance gap. Additionally, pre-reduction of NiO to Ni during operation enhances porosity, improving TPB

accessibility. This sustainable approach offers a promising pathway toward environmentally friendly, not only for high-performance SOFC but also for other perovskite material-based applications.

Conflicts of interest

The authors declare no conflict of interest.

Data availability

The data will be made available upon request.

Acknowledgements

References

1 O. Chun, *et al.*, Advances in low-temperature solid oxide fuel cells: An explanatory review, *J. Power Sources*, 2024, **610**, 234719.

2 M. A. Azni, *et al.*, Review of the effects of fossil fuels and the need for a hydrogen fuel cell policy in Malaysia, *Sustainability*, 2023, **15**(5), 4033.

3 H. Hou, *et al.*, Exploring the Role of Fossil Fuels and Renewable Energy in Determining Environmental Sustainability: Evidence from OECD Countries, *Sustainability*, 2023, **15**(3), 2048.

4 S. Christian, Additive manufacturing of solid oxide fuel cells. A comprehensive review of patent literature, *J. Power Sources*, 2025, **625**, 235702.

5 Y. Hu, *et al.*, Recent progress of high-performance interconnectors for SOFC: From materials, protective coatings, optimizing strategies, towards the real stack applications, *Chem. Eng. J.*, 2025, **505**, 159321.

6 X. Haoran, *et al.*, Status and progress of metal-supported solid oxide fuel cell: Towards large-scale manufactory and practical applications, *Energy Rev.*, 2024, **3**(1), 100051.

7 S. Kazula, S. de Graaf and L. Enghardt, Review of fuel cell technologies and evaluation of their potential and challenges for electrified propulsion systems in commercial aviation, *J. Glob. Power Propuls. Soc.*, 2023, **7**, 43–57.

8 M. R. Gao, *et al.*, Strategic Design of "Three-in-One" Cathode Toward Optimal Performance of Proton-Conducting Solid Oxide Fuel Cell: The Temperature Matters, *Carbon Energy*, 2025, e683.

9 S. E. Wolf, *et al.*, Internal biogas reforming in solid oxide and proton conducting ceramic cells: Progress, challenges and perspectives, *J. Phys.: Energy*, 2025, **7**(2), 021002.

10 C. Duan, *et al.*, Proton-conducting oxides for energy conversion and storage, *Applied Physics Reviews*, 2020, **7**(1), 011314.

11 C. Jiafeng, *et al.*, Recent advances and perspectives of fluorite and perovskite-based dual-ion conducting solid oxide fuel cells, *J. Energy Chem.*, 2021, **57**, 406–427.

12 J. Kim, *et al.*, Proton conducting oxides: A review of materials and applications for renewable energy conversion and storage, *Renewable Sustainable Energy Rev.*, 2019, **109**, 606–618.

13 M. K. Hossain, *et al.*, Recent progress in barium zirconate proton conductors for electrochemical hydrogen device applications: A review, *Ceram. Int.*, 2021, **47**(17), 23725–23748.

14 M. Yu, *et al.*, Recent Novel Fabrication Techniques for Proton-Conducting Solid Oxide Fuel Cells, *Crystals*, 2024, **14**(3), 225.

15 I. T. Bello, *et al.*, Scientometric review of proton-conducting solid oxide fuel cells, *Int. J. Hydrogen Energy*, 2021, **46**(75), 37406–37428.

16 S. J. Heo, *et al.*, Mn Additive Improves Zr Grain Boundary Diffusion for Sintering of a Y-Doped BaZrO3 Proton Conductor, *ACS Appl. Mater. Interfaces*, 2024, **16**(9), 11646–11655.

17 S. Dwivedi, Solid oxide fuel cell: Materials for anode, cathode and electrolyte, *Int. J. Hydrogen Energy*, 2020, **45**(44), 23988–24013.

18 J. T. S. Irvine, Perovskite oxide anodes for SOFCs, *Perovskite Oxide For Solid Oxide Fuel Cells*, 2009, pp. 167–182.

19 A. N. Zainon, *et al.*, Challenges in using perovskite-based anode materials for solid oxide fuel cells with various fuels: a review, *Int. J. Hydrogen Energy*, 2023, **48**(53), 20441–20464.

20 J. Zhao, *et al.*, Efficient ferrite-based perovskite anode for solid oxide fuel cells with A-site and B-site co-exsolution, *Energy Fuels*, 2020, **34**(8), 10100–10108.

21 E. Fabbri, D. Pergolesi and E. Traversa, Electrode materials: a challenge for the exploitation of protonic solid oxide fuel cells, *Sci. Technol. Adv. Mater.*, 2010, **11**(4), 044301.

22 B. H. Rainwater, M. Liu and M. Liu, A more efficient anode microstructure for SOFCs based on proton conductors, *Int. J. Hydrogen Energy*, 2012, **37**(23), 18342–18348.

23 S. H. Hwang, *et al.*, Fabrication of an electrolyte-supported protonic ceramic fuel cell with nano-sized powders of Ni-composite anode, *Int. J. Hydrogen Energy*, 2021, **46**(1), 1076–1084.

24 Y. Zhang, *et al.*, Understanding of redox behavior of Ni–YSZ cermets, *Solid State Ionics*, 2009, **180**(36–39), 1580–1586.

25 Y.-H. Heo, *et al.*, Redox-induced performance degradation of anode-supported tubular solid oxide fuel cells, *Int. J. Hydrogen Energy*, 2011, **36**(1), 797–804.

26 M. Fallah Vostakola and B. A. Horri, Progress in Material Development for Low-Temperature Solid Oxide Fuel Cells: A Review, *Energies*, 2021, **14**(5), 1280.

27 J. Laurencin, *et al.*, Solid oxide fuel cells damage mechanisms due to Ni-YSZ re-oxidation: case of the anode supported cell, *J. Power Sources*, 2009, **192**(2), 344–352.

28 O. Gohar, *et al.*, Nanomaterials for advanced energy applications: Recent advancements and future trends, *Mater. Des.*, 2024, **241**, 112930.

29 M. Irshad, *et al.*, A brief description of high temperature solid oxide fuel cell's operation, materials, design, fabrication technologies and performance, *Appl. Sci.*, 2016, **6**(3), 75.

30 S.-W. Baek and J. Bae, Anodic behavior of 8Y2O3–ZrO2/NiO cermet using an anode-supported electrode, *Int. J. Hydrogen Energy*, 2011, **36**(1), 689–705.

31 A. Nenning, *et al.*, A novel approach for analyzing electrochemical properties of mixed conducting solid oxide fuel cell anode materials by impedance spectroscopy, *Phys. Chem. Chem. Phys.*, 2014, **16**(40), 22321–22336.

32 K. Ng, H. Rahman and M. Somalu, Enhancement of composite anode materials for low-temperature solid oxide fuels, *Int. J. Hydrogen Energy*, 2019, **44**(58), 30692–30704.

33 A. N. Zainon, *et al.*, Challenges in using perovskite-based anode materials for solid oxide fuel cells with various fuels: a review, *Int. J. Hydrogen Energy*, 2023, **48**(53), 20441–20464.

34 B. Timurkutluk and E. Ucar, A route for enhancing the performance of solid oxide fuel cell anodes produced from commercial powders, *J. Power Sources*, 2025, **625**, 235715.

35 U. Aarthi and K. S. Babu, Grain boundary space charge modulation in BaZr0.8Y0.2-xMxO3−δ with transition metal (M= Ni, Co, Fe, and Zn) co-doping, *Int. J. Hydrogen Energy*, 2020, **45**(53), 29356–29366.

36 K.-R. Lee, *et al.*, Fabrication of anode-supported thin BCZY electrolyte protonic fuel cells using NiO sintering aid, *Int. J. Hydrogen Energy*, 2019, **44**(42), 23784–23792.

37 H. S. Soares, *et al.*, Effect of the addition mechanism of ZnO sintering aid on densification, microstructure and electrical properties of Ba(Zr,Y)O3-δ proton-conducting perovskite, *Int. J. Hydrogen Energy*, 2021, **46**(52), 26466–26477.

38 Q. u. Ain, *et al.*, Towards sustainable electrochemistry: green synthesis and sintering aid modulations in the development of BaZr0. 87Y0. 1M0. 03O3− δ (M= Mn, Co, and Fe) IT-SOFC electrolytes, *Front. Chem.*, 2023, **11**, 1322475.

39 L. Zhang, *et al.*, New BaZr0. 125Y0. 125M0. 75O3 (M= Cu, Mn, Ni, Zn, Co, and Fe) cathodes for proton-conducting solid oxide fuel cells, *Int. J. Hydrogen Energy*, 2024, **71**, 1214–1221.

40 K.-Y. Park, *et al.*, Enhanced proton conductivity of yttrium-doped barium zirconate with sinterability in protonic ceramic fuel cells, *J. Alloys Compd.*, 2015, **639**, 435–444.

41 M. L. Tummino, *et al.*, Sucrose-Assisted Solution Combustion Synthesis of Doped Strontium Ferrate Perovskite-Type Electrocatalysts: Primary Role of the Secondary Fuel, *Catalysts*, 2020, **10**(1), 134.

42 J. E. Hutchison, Greener nanoscience: a proactive approach to advancing applications and reducing implications of nanotechnology, *ACS Nano*, 2008, **2**(3), 395–402.

43 M. R. Kalaie, *et al.*, Preparation and characterization of superparamagnetic nickel oxide particles by chemical route, *Appl. Nanosci.*, 2016, **6**(6), 789–795.

44 M. Irshad, *et al.*, Evaluation of BaZr0. 8X0. 2 (X= Y, Gd, Sm) proton conducting electrolytes sintered at low temperature for IT-SOFC synthesized by cost effective combustion method, *J. Alloys Compd.*, 2020, **815**, 152389.

45 M. Chen, *et al.*, Densification and electrical conducting behavior of BaZr0. 9Y0. 1O3-δ proton conducting ceramics with NiO additive, *J. Alloys Compd.*, 2019, **781**, 857–865.

46 R. I. Muneeb Irshad, K. Siraj, I. Shakir, M. Rafique, Q. ul Ain and R. Raza, Electrochemical evaluation of mixed ionic electronic perovskite cathode LaNi1-xCoxO3-δ for IT-SOFC synthesized by high temperature decomposition, *Int. J. Hydrogen Energy*, 2021, **46**(17), 10448–10456.

47 X. Fu, *et al.*, Novel solid–solid phase change materials with biodegradable trihydroxy surfactants for thermal energy storage, *RSC Adv.*, 2015, **5**(84), 68881–68889.

48 C. S. Jincy and P. Meena, Evaluation of cytotoxic activity of Fe doped cobalt oxide nanoparticles, *J. Trace Elem. Med. Biol.*, 2022, **70**, 126916.

49 M. Ahsan, *et al.*, The effect of calcination temperature on the properties of Ni-SDC cermet anode, *Ceram. Int.*, 2020, **46**(3), 2780–2785.

50 T. Ghorbani-Moghadam, A. Kompany and M. Golmohammad, The comparative study of doping Cu and Fe on the cathodic properties of La0. 7Sr1. 3CoO4 layered perovskite compound: To be used in IT-SOFC, *J. Alloys Compd.*, 2022, **926**, 166928.

51 C. B. Njoku and P. G. Ndungu, Synthesis and characterization of novel Ce0. 8Sm0. 2Fe0. 9Ir0. 03Co0. 07O3− δ perovskite material and possible application as a cathode for low–intermediate temperature SOFCs, *Mater. Res. Bull.*, 2015, **68**, 100–108.

52 J. Al Boukhari, A. Khalaf and R. Awad, Structural analysis and dielectric investigations of pure and rare earth elements (Y and Gd) doped NiO nanoparticles, *J. Alloys Compd.*, 2020, **820**, 153381.

53 M. Irshad, *et al.*, Investigating the microstructural and electrochemical performance of novel La 0.3 Ba 0.7 Zr 0.5 X 0.3 Y 0.2 (X= Gd, Mn, Ce) electrolytes at intermediate temperature SOFCs, *Sustainable Energy Fuels*, 2022, **6**(23), 5384–5391.

54 M. Irshad, *et al.*, Evaluation of highly conductive cermet cathodes synthesized with organic chelating agents and sintered at low temperatures for IT-SOFCs, *Energy Convers. Manage.:X*, 2024, **23**, 100609.

55 M. K. Muneeb Irshad, M. Rafique, N. Ahmad, K. Siraj, R. Raza, M. Sadiq, M. Ahsan, A. Ghaffarg and A. Ashfaq, Evaluation of BaCo0.4Fe0.4Zr0.2−xNixO3−δ perovskite cathode using nickel as a sintering aid for IT-SOFC, *RSC Adv.*, 2021, **11**, 14475–14483.